

Elastic electron scattering from ^{17}Ne and ^{27}P exotic nuclei

A. K. Hamoudi, R. A. Radhi, A. R. Ridha

Department of Physics, College of Science, University of Baghdad, Baghdad, Iraq

E-mail: Email: arkan_rifaah@yahoo.com

Abstract

The ground state proton, neutron and matter densities and corresponding root mean square radii of unstable proton-rich ^{17}Ne and ^{27}P exotic nuclei are studied via the framework of the two-frequency shell model. The single particle harmonic oscillator wave functions are used in this model with two different oscillator size parameters b_{core} and b_{halo} , the former for the core (inner) orbits whereas the latter for the halo (outer) orbits. Shell model calculations for core nucleons and for outer (halo) nucleons in exotic nuclei are performed individually via the computer code OXBASH. Halo structure of ^{17}Ne and ^{27}P nuclei is confirmed. It is found that the structure of ^{17}Ne and ^{27}P nuclei have $(1d_{5/2})^2$ and $2s_{1/2}$ -dominant configurations, respectively. Elastic electron scattering form factors of these exotic nuclei are also studied using the plane wave Born approximation. Effects of the long tail behavior of the proton density distribution on the proton form factors of ^{17}Ne and ^{27}P are analyzed. It is found that the difference between the proton form factor of ^{17}Ne and that of stable ^{20}Ne (or of ^{27}P and that of stable ^{31}P) comes from the difference in the proton density distribution of the last two protons (or of the last proton) in the two nuclei. It is concluded that elastic electron scattering will be an efficient tool (in the near future) to examine proton-halo phenomena of proton-rich nuclei.

Key words

proton-rich exotic nuclei, shell model calculations, elastic electron scattering, form factor, matter and proton density distributions.

Article info.

Received: Jun. 2015

Accepted: Oct. 2015

Published: Dec. 2015

الأستطارة الألكترونية المرنة من النوى الغريبة ^{17}Ne و ^{27}P

عادل خلف حمودي، رعد عبد الكريم راضي، اركان رفعة رضا

قسم الفيزياء، كلية العلوم، جامعة بغداد، بغداد، العراق

الخلاصة

تم دراسة توزيعات الكثافة البروتونية والنيوترونية والكتلية بالإضافة الى أنصاف الأقطار المقابلة لها للنواتين غير المستقرتين الغنيتين بالبروتونات ^{17}Ne و ^{27}P من خلال أنموذج القشرة ذو معلمي التردد. تم أستخدام الدوال الموجية للمتذبذب التوافقي للجسيمة المفردة في هذا الأنموذج مع قيمتين مختلفتين للثابت التوافقي b_{halo} و b_{core} ، السابق لمدارات القلب (الداخلي) بينما الأخير لمدارات الهالة (الخارجي). حسابات أنموذج القشرة لنيوكليونات القلب وللنيوكليونات الخارجية (الهالة) للنواتين الغريبتين تمت على انفراد من خلال برنامج أوكسباش (Oxbash). أكد تركيب الهالة للنواتين ^{17}Ne و ^{27}P . وجد بأن تركيب النواتين ^{17}Ne و ^{27}P لها التشكيلات المهيمنة $(1d_{5/2})^2$ و $2s_{1/2}$ على التوالي. كما وتم دراسة عوامل التشكل للأستطارة الألكترونية المرنة لهاتين النواتين الغريبتين بأستخدام تقريب بورن للموجة المستوية. وتم تحليل تأثير سلوك المركبة الطويلة لتوزيع الكثافة البروتونية على عوامل التشكل البروتونية للنواتين ^{17}Ne و ^{27}P . ووجد بأن الأختلاف بين عوامل التشكل ^{17}Ne وتلك المحسوبة ^{20}Ne (أو ^{27}P وتلك للنواة المستقرة ^{31}P) يأتي من الأختلاف في توزيع الكثافة البروتونية للبروتونين الأخيرين (أو للبروتون الأخير) في كلا النواتين. يستنتج مما سبق بأن الأستطارة الألكترونية المرنة ستكون أداة فعالة (في المستقبل القريب) لأختبار ظواهر هالة-البروتون للنوى الغنية بالبروتونات.

Introduction

The detection of the neutron halo (in 1985) in exotic neutron-rich nuclei, investigations on halo phenomena [1-4] have grown to be a hot subject in nuclear physics. Halo nuclei have extraordinary large root mean square (rms) radii of matter density distribution. The reason of occurrence of the halo phenomenon is attributed to both of; the small separation energy of the outer few nucleons and their occupation on orbits with low angular momentum. Numerous experiments [5-7] were carried out to investigate the neutron halo in neutron-rich nuclei, where neutron halo nuclei are well recognized in the region of light mass. Theoretically, different models [8-13] were used to study the neutron halo in exotic nuclei ${}^6,8\text{He}$, ${}^{11}\text{Li}$, ${}^{11,14}\text{Be}$, ${}^{17}\text{B}$ and ${}^{19}\text{C}$.

While the neutron halo was well studied in neutron-rich nuclei, investigations on proton halo are comparatively less. Theoretically, many attempts were made to look for proton halo in proton drip-line nuclei. Calculations using different models [14, 15] demonstrate that there may be proton halo in the ground state of ${}^{26-27}\text{P}$, ${}^8\text{B}$, ${}^{17}\text{Ne}$ and in the excited state of ${}^6\text{Li}$ and ${}^{17}\text{F}$. The occurrence of the proton halo in ${}^{26}\text{P}$ and ${}^{27}\text{S}$ was firstly predicted by Ren et al. [14]. Brown and Hansen [15] also studied the halo phenomena in ${}^{26-27}\text{P}$ and ${}^{26-28}\text{S}$ isotopes and found that these isotopes are well applicants for proton halo nuclei. Experiments [16-20] as well demonstrate some signs of the presence of proton halo in these nuclei. However, more experiments are required to verify the presence of the proton halo.

The proton drip-line nucleus ${}^{17}\text{Ne}$ is an attractive but relatively poorly studied system. It has a Borromean binding structure, where none of the

binary subsystems (${}^{15}\text{O} + p + p$) are bound. The ${}^{17}\text{Ne}$ nucleus has attracted attention as well because of the possibility of two proton emission from excited states [21]. The two proton halo structure of ${}^{17}\text{Ne}$ was originally suggested by Zhukov and Thompson [22]. Recently, Tanaka et al. [23] have deduced the density distribution of ${}^{17}\text{Ne}$ from their measurement of reaction cross sections through a modified Glauber-type model, they have indicated that ${}^{17}\text{Ne}$ has a long tail in the density and a $(2s_{1/2})^2$ -dominant configuration of two outer protons. Outcomes of theoretical studies of ${}^{17}\text{Ne}$ are controversial. Calculations of Refs [24, 25] indicate that the structure of ${}^{17}\text{Ne}$ has a $(2s_{1/2})^2$ -dominant configuration. The three-body model calculations carried out by Garrido et al. [26, 27] suggest that there are almost equal occupation probabilities of $(2s_{1/2})^2$ and $(1d_{5/2})^2$ levels. Calculations of Fourtune et al. [28, 29] suggest that the structure of ${}^{17}\text{Ne}$ has a $(1d_{5/2})^2$ -dominant configuration. Moreover, calculations of reaction cross sections, using a Hartree-Fock type wave function and Glauber model, performed by Kitagawa et al. [30] also propose that the structure of ${}^{17}\text{Ne}$ has a $(1d_{5/2})^2$ -dominant configuration.

The current experimental technique for recognizing neutron halo and proton halo are mostly based on the measurement of reaction cross sections of the nucleus-nucleus collision and of the momentum distributions of nucleus breakup. There are complex processes where the strong and electromagnetic interactions among nucleons play a role. Despite the fact that this type of experiments has achieved most important success for halo phenomena,

it is motivating to look for a new probe to refine the study of proton halo in proton rich-nuclei. Electron-nucleus scattering has confirmed to be a tremendous tool for the study of nuclear structure, particularly for the study of electromagnetic properties of nuclei. It has given much consistent information on proton density distributions of stable nuclei. The physics of this process is very simple because the electromagnetic interaction is the only interaction found between an electron and target nucleus. Therefore, we regard that the electron-nucleus scattering is a better technique for the accurate study of the long tail behavior presented in the proton density distribution of the exotic proton-rich nuclei. However, electron scattering on exotic nuclei was not feasible in the past because of the complexity of manufacture targets from unstable nuclei. The construction of new colliders of electron and unstable nucleus at RIKEN in Japan [31] and at GSI in Germany [32] will give a good opportunity to investigate the proton density distributions of unstable exotic nuclei by elastic electron scattering. Thus, it is motivating to do an exploratory study of elastic electron scattering from proton-rich nuclei.

There has been no detailed study of elastic electron scattering, in terms of the two frequency shell-model, on unstable proton-rich exotic nuclei. We thus, in the present study, investigate the proton form factor of ^{17}Ne and ^{27}P exotic nuclei through combining the proton density distribution, obtained by the two-frequency shell model, with the plane wave Born approximation. Effects of the long tail behavior of the proton density distribution on the proton form factors of ^{17}Ne and ^{27}P exotic nuclei are investigated. We find that the

difference between the proton form factor of ^{17}Ne and that of stable ^{20}Ne (or of ^{27}P and that of stable ^{31}P) comes from the difference in the proton density distribution of the last two protons (or of the last proton) in the two nuclei. We confirm the halo structure of ^{17}Ne and ^{27}P nuclei and find that their structures have $(1d_{5/2})^2$ and $2s_{1/2}$ -dominant configurations, respectively.

Theory

The one-body operator of the longitudinal transition density for point protons (with isospin $t_z = 1/2$) or neutrons ($t_z = -1/2$) is given by [33]

$$\hat{\rho}_{\Delta J, t_z}^L = \sum_{k=1}^A e(t_z) \frac{\delta(r - r_k)}{r_k^2} Y_{\Delta J, M_{\Delta J}}(\Omega_{r_k}), \quad (1)$$

with

$$e(t_z) = \frac{1 + 2t_z(k)}{2}.$$

In Eq. (1), L is written above the operator $\hat{\rho}_{\Delta J, t_z}^L$ to remind us that we use a longitudinal operator, $Y_{\Delta J, M_{\Delta J}}(\Omega_{r_k})$ and $\delta(\vec{r} - \vec{r}_k)$ are the spherical harmonic and Dirac delta functions, respectively. Finally, r_k and Ω_{r_k} represent position and solid angle for k 's nucleon in position coordinate. The multipolarity ΔJ of the transition is restricted by the following angular momentum and parity selection rules:

$$|J_i - J_f| \leq \Delta J \leq J_i + J_f$$

and

$$\pi_i \pi_f = (-1)^{\Delta J} \quad (\text{for Coulomb transitions}).$$

The reduced matrix element of the longitudinal transition density operator, Eq. (1), can now be expressed as [33]

$$\langle J_f \| \hat{\rho}_{\Delta J, t_z}^L(\vec{r}) \| J_i \rangle = \frac{1}{\sqrt{4\pi(2J_i + 1)}} \sum_{ab} OBDM(J_f, J_i, \Delta J, a, b, t_z) \langle j_a \| Y_{\Delta J} \| j_b \rangle R_{n_a}^{l_a}(r) R_{n_b}^{l_b}(r), \quad (2)$$

where a and b label single-particle states for the considered shell model space and are specified by

$$|p\rangle = |n_p l_p\rangle |j_p m_p\rangle, \quad (\text{the state } p \text{ represents either a or b}).$$

The states $|J_i\rangle$ and $|J_f\rangle$ are characterized by the model space wave functions. In Eq. (2), $R_{n_p l_p}(r)$ is the radial part of the harmonic oscillator wave function, $\langle j_a \| Y_{\Delta J} \| j_b \rangle$ is the reduced matrix element of the spherical harmonic and $OBDM(J_f, J_i, \Delta J, a, b, t_z)$ is the proton ($t_z = 1/2$) or neutron ($t_z = -1/2$) one body density matrix

element given by the second quantization as [33]

$$OBDM(J_f, J_i, \Delta J, a, b, t_z) = \frac{\langle J_f \| [a_{a, t_z}^+ \otimes \tilde{a}_{b, t_z}]^{\Delta J} \| J_i \rangle}{\sqrt{2\Delta J + 1}}. \quad (3)$$

As the *spsdpf*-, *sd*- and *p*-shell wave functions (generated in the present study with WBP [34], USD [35] and CKI [36] interactions, respectively) have good isospin, it is appropriate to evaluate the *OBDM* elements by means of isospin-reduced matrix elements. The relation between these triply reduced *OBDM* and the proton or neutron *OBDM* of Eq. (2) is given by

$$OBDM(t_z) = (-1)^{T_f - T_z} \sqrt{2} \begin{pmatrix} T_f & 0 & T_i \\ -T_z & 0 & T_z \end{pmatrix} OBDM(\Delta T = 0) / 2 + 2t_z (-1)^{T_f - T_z} \sqrt{6} \begin{pmatrix} T_f & 1 & T_i \\ -T_z & 0 & T_z \end{pmatrix} OBDM(\Delta T = 1) / 2 \quad (4)$$

where T_i and T_f are the total initial and final isospin of the nuclear system under study. T_z is the projection of the total isospin and is given by $T_z = \frac{Z - N}{2}$ where Z and N are the atomic and neutron numbers of the

nuclear system under study. These triply reduced *OBDM*(ΔT) (*OBDM*($\Delta T = 0$) is called isoscalar and *OBDM*($\Delta T = 1$) is called isovector) elements in Eq. (4) are given in terms of the second quantization as

$$OBDM(f, \Delta J, \alpha, \beta, \Delta T) = \frac{\langle \Gamma_f \| [a_{\alpha}^+ \otimes \tilde{a}_{\beta}]^{\Delta J, \Delta T} \| \Gamma_i \rangle}{\sqrt{2\Delta J + 1} \sqrt{2\Delta T + 1}} \quad (5)$$

Here, Greek symbols are utilized to indicate quantum numbers in coordinate space and isospace (i.e., $\Gamma_i \equiv J_i T_i$ and $\Gamma_f \equiv J_f T_f$).

The *OBDM*(ΔT) elements contain all of the information about transitions of given multiplicities which are embedded in the model wave

functions. To obtain these *OBDM* elements, we perform shell model calculations using realistic effective interactions.

For the ground state density distribution, we have $J_i = J_f$, $\Delta J = 0$. Therefore, Eq. (2) becomes as

$$\rho_{t_z}(r) = \frac{1}{\sqrt{4\pi(2J_i + 1)}} \sum_{ab} OBDM(J_i, J_i, 0, a, b, t_z) \langle j_a \| Y_0 \| j_b \rangle R_{n_a}(r) R_{n_b}(r), \quad (6)$$

where

$$\rho_{t_z}(r) = \langle J_i \| \hat{\rho}_{\Delta J=0, t_z}^L(\vec{r}) \| J_i \rangle.$$

As halo nuclei, which are our investigated subject of the present study, are oversized and easily broken systems consisting of a compact core plus a number of outer nucleons loosely bound and spatially extended far from the core, it is suitable to separate the ground state density distribution of Eq. (6) into two parts. The first part is connected to the core nucleons while the second is connected to the halo (outer) nucleons, i.e.

$$\rho_m(r) = \rho^{core}(r) + \rho^{halo}(r). \quad (7)$$

Moreover, Eq. (6) may also be expressed as

$$\rho_m(r) = \rho_p(r) + \rho_n(r), \quad (8)$$

where $\rho_p(r)$ and $\rho_n(r)$ are the ground state proton and neutron densities of halo nuclei expressed as

$$\rho_p(r) = \rho_p^{core}(r) + \rho_p^{halo}(r) \quad (9)$$

and

$$\rho_n(r) = \rho_n^{core}(r) + \rho_n^{halo}(r). \quad (10)$$

The normalization condition of the above ground state densities is given by

$$g = 4\pi \int_0^\infty \rho^g(r) r^2 dr. \quad (11)$$

Here, $\rho^g(r)$ represents one of the following densities: $\rho_m(r)$, $\rho^{core}(r)$, $\rho^{halo}(r)$, $\rho_p(r)$, $\rho_n(r)$. In that case, the parameter g [presented in the L.H.S. of Eq. (11)] represents, correspondingly, one of the following quantities: the nuclear mass (A), the number of core nucleons, the number of halo nucleons, the total number of protons and the total number of neutrons of halo nuclei. The rms radii

of corresponding above densities are given by

$$\langle r^2 \rangle_g^{1/2} = \frac{4\pi}{g} \int_0^\infty \rho^g(r) r^4 dr. \quad (12)$$

Next we use the plane wave Born approximation (PWBA) to study the elastic electron scattering form factors from considered nuclei. In the PWBA, the incident and scattered electron waves are represented by plane waves. The elastic proton form factor is simply given by the Fourier-Bessel transform of the ground state proton density distribution, i.e.

$$F(q) = \frac{4\pi}{Z} \int_0^\infty \rho_p(r) j_0(qr) r^2 dr \quad (13)$$

where $j_0(qr)$ is the spherical Bessel function of order zero and q is the momentum transfer from the incident electron to the target nucleus.

In the limit $q \rightarrow 0$, the target nucleus will be characterized as a point particle. Accordingly, using Eq. (13) with the help of Eq. (9), the proton form factor of this target nucleus will be equal to unity (i.e. $F(q \rightarrow 0) = 1$).

Results and discussion

The method of two-frequency shell model [37] is employed to study the ground state proton, neutron and matter density distributions, the root mean square proton, neutron and matter radii and elastic proton form factors of unstable ^{17}Ne ($J^\pi, T = 1/2^-, 3/2$) and ^{27}P ($J^\pi, T = 1/2^+, 3/2$) nuclei. The single particle harmonic oscillator wave functions are used with two different oscillator size parameters b_{core} and b_{halo} . In this study, both b_{core} and b_{halo} are considered as free parameters to be adjusted so as to reproduce the experimental root mean square radii of

core and halo (exotic) nuclei, respectively. To obtain the one body density matrix (OBDM) elements and occupation numbers of states for core and halo parts (required for calculations of the core and halo densities), we perform shell model calculations via the computer code OXBASH [38].

Shell model calculations for ^{15}O -core and for the outer (halo) two protons in ^{17}Ne are performed individually in $1p$ and $2s1d$ -model spaces, respectively. Realistic interactions of Cohen-Kurath (CKI) [36] and Brown-Wildenthal (USD) [35] are used for the ^{15}O -core and for the outer two protons, respectively. For ^{26}Si -core of ^{27}P , we perform shell model calculations in the $spsdpf$ -model space with $0\hbar\omega$ truncations using the realistic interaction of WBP [34]. Here, we consider a simple calculation by assuming that the orbits $1s_{1/2}$, $1p_{3/2}$ and $1p_{1/2}$ are filled while the orbit $1d_{5/2}$ is occupied by 10 nucleons (6 protons and 4 neutrons). However, the outer (halo) proton in ^{27}P is assumed to occupy the orbit $2s_{1/2}$.

The proton drip-line ^{17}Ne has a Borromean binding structure. The outer two protons are weakly bound ($S_{2p} = 0.93$ MeV). To reproduce the experimental root mean square radii of ^{15}O -core and halo nucleus ^{17}Ne , we choose values for oscillator size parameters $b_{core} = 1.61$ fm and $b_{halo} = 2.63$ fm. The calculated rms matter radius of ^{15}O is 2.406 fm, in agreement with the experimental value of 2.44 ± 0.04 fm [39]. The calculated rms proton, neutron and matter radii of ^{17}Ne nucleus are 3.084 fm, 2.394 fm and 2.821 fm, respectively while those of experimental data [40] are,

correspondingly, 2.97 ± 0.07 fm, 2.69 ± 0.07 fm and 2.75 ± 0.07 fm. The comparison demonstrates a reasonable agreement between the calculated and the experimental rms radii of ^{17}Ne . The difference between the calculated overall proton and neutron rms radii is 0.690 fm. This difference indicates a definite degree of halo structure.

For ^{27}P , the outer proton is inadequately bound ($S_p = 0.9$ MeV). Here, we select values for $b_{core} = 1.785$ fm and $b_{halo} = 3.25$ fm. Our calculations give result of 2.949 fm for the rms matter radius of ^{26}Si -core nucleus. The calculated rms proton, neutron and matter radii of ^{27}P are 3.278, 2.915 and 3.122 fm whereas those of experimental data [17] are, respectively, 3.220 ± 0.163 , 2.754 ± 0.14 and 3.020 ± 0.155 fm. The comparison shows a good agreement between the calculated rms radii and those of experimental one. The difference between the calculated overall proton and neutron rms radii is 0.363 fm. This difference gives a sign for the existence of the halo structure in ^{27}P nucleus.

The matter density $\rho_m(r)$ (in fm^{-3}) of ^{17}Ne and ^{27}P are plotted, respectively, in Figs. 1(a) and 1(b) as a function of r (in fm). In Fig. 1(a), the solid line is the calculated matter density obtained with the assumption that the outer two protons in ^{17}Ne move in the $2s1d$ -model space. Here, the OBDM elements of the outer two protons (needed for calculations of the halo density) are calculated by means of the realistic interaction USD [35]. The dashed and dash-dotted lines are the calculated matter densities when the outer two protons are in the pure $1d_{5/2}$ and pure $2s_{1/2}$, respectively. The filled circles are the experimental

matter densities deduced from the Glauber model using the fitting procedure with (HO+HO) density function [23]. It is clear that both the solid and the dashed distributions, in which their behavior is nearly the same throughout the whole range of the data, are better in describing the fitted data than the dash-dotted one. Besides, the long tail behavior, which is a distinctive feature of halo nuclei, is evidently revealed in these calculated distributions. The ground state occupation numbers of the outer two protons in ^{17}Ne , obtained by the $2s1d$ -shell model calculations using the realistic interaction of USD, are 1.579, 0.120 and 0.301 for $(1d_{5/2})^2$, $(1d_{3/2})^2$ and $(2s_{1/2})^2$ configurations, respectively. Inspection of these occupation numbers and also of calculated matter densities shown in Fig. 1(a) leads to the conclusion that the structure of the ^{17}Ne nucleus has a $(1d_{5/2})^2$ -dominant configuration. This dominancy, in agreement with the studies [28-30], may be attributed to

the change of the shell structure in the proton-rich ^{17}Ne nucleus (i.e., the level inversion between $2s_{1/2}$ and $1d_{5/2}$) as suggested by Ref [23].

In Fig. 1(b), the ground state matter density distribution of ^{27}P is calculated by assuming that the outer proton moves in the pure $2s_{1/2}$ (denoted by the solid line). The fitted to the experimental matter densities (denoted by filled circles) [41], deduced from the Glauber model with HO-type core plus Yukawa-square tail for the proton density distribution, are also displayed in this figure for comparison. Again the long tail behavior, which is a distinguishing signal of halo nuclei, is markedly exposed in the solid line. This gives an indication that the structure of the ^{27}P nucleus has a $2s_{1/2}$ -dominant configuration. Moreover, the solid distribution shows a good agreement with the fitted to the experimental one throughout the whole range of the data.

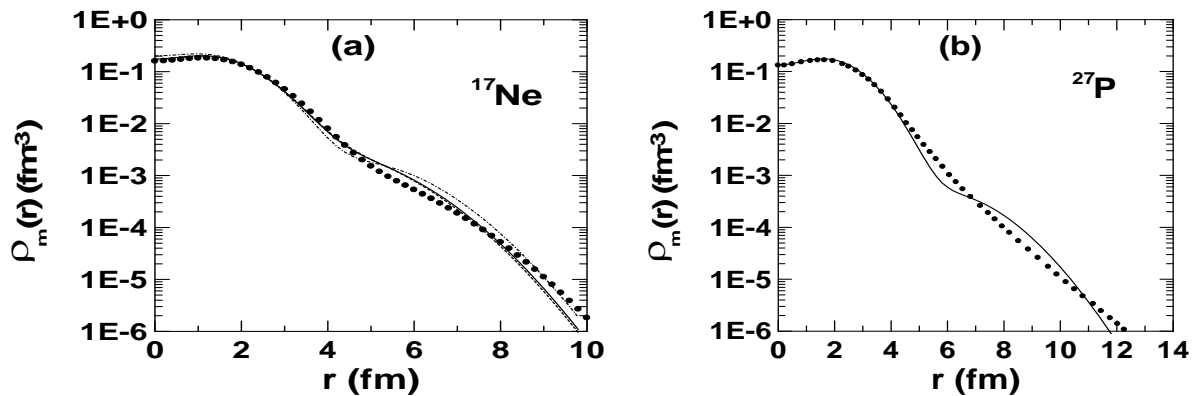


Fig.1: The dependence of matter density distributions (in fm^{-3}) of ^{17}Ne (a) and ^{27}P (b) on r (in fm). In (a), the solid line corresponds to the density calculated when the outer two protons in ^{17}Ne move within the sd -model space, the dashed and dash-dotted lines correspond to densities calculated when the outer two protons move in the pure $1d_{5/2}$ and pure $2s_{1/2}$, respectively. In (b), the solid line corresponds to the density calculated when the outer proton in ^{27}P moves in the pure $2s_{1/2}$. The filled circles in (a) and (b) correspond to experimental densities deduced from Glauber model by Refs. [23] and [41], respectively.

In Fig. 2(a), we repeat the calculations exactly as in Fig. 1(a) but this time for the proton $\rho_p(r)$ and neutron $\rho_n(r)$ density distributions of ^{17}Ne . The solid, dashed and dash-dotted lines are the calculated proton density distributions of ^{17}Ne when the outer two protons move in the $2s1d$ -model space, pure $1d_{5/2}$ and pure $2s_{1/2}$, respectively. The plus symbols are the calculated neutron density distribution. It is clear that the performance of the solid, dashed and dash-dotted distributions shown in Fig.2(a) is almost identical along all range of considered r . For a second time, the long tail behavior (which is a characteristic mark of halo nuclei) is noticeably seen in these distributions of proton densities. This behavior is related to the existence of the outer two protons of ^{17}Ne in the halo orbits.

In Fig. 2(b), we do again calculations precisely as in Fig. 1(b)

but now for the proton $\rho_p(r)$ and neutron $\rho_n(r)$ distributions of ^{27}P . The solid distribution is the calculated proton density distribution when the outer proton of ^{27}P moves in the pure $2s_{1/2}$. The plus symbols are the calculated neutron density distribution. Once more, the long tail behavior is apparently seen in the solid distribution of the proton density. This behavior is associated to the existence of the outer proton of ^{27}P in the halo orbits.

The calculated neutron $\rho_n(r)$ density distributions of ^{17}Ne and ^{27}P shown in Figs. 2(a) and 2(b) demonstrate a steep slope behavior because there are no neutrons found in the halo orbits (all neutrons of ^{17}Ne and ^{27}P are found within their core only). It is useful to remark that the halo phenomenon in ^{17}Ne and ^{27}P is connected to the matter and proton densities but not to the neutron density.

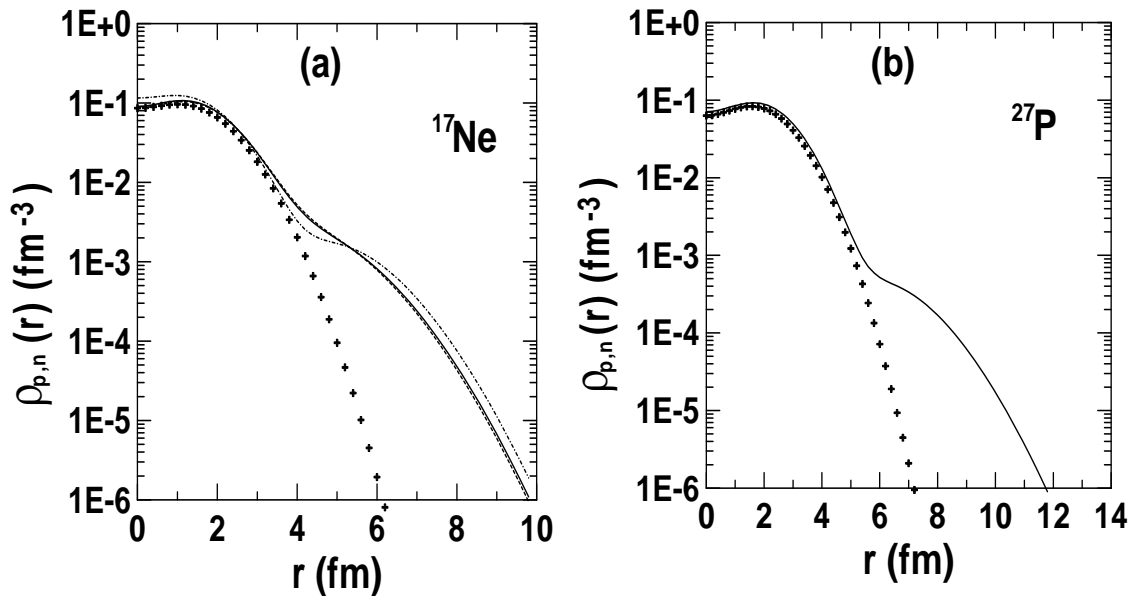


Fig. 2: The dependence of proton and neutron density distributions (in fm^{-3}) of ^{17}Ne (a) and ^{27}P (b) on r (in fm). In (a), the solid, dashed and dash-dotted lines are the same as those of Fig. 1 (a) but for the calculated proton density distributions. In (b), the solid line is the same as that of Fig. 1 (b) but for the calculated proton density distribution. In (a) and (b), the plus symbols are the neutron densities of unstable proton-rich ^{17}Ne and ^{27}P nuclei.

In Figs. 3(a) and 3(b), we present the proton density distributions of $^{20,17}\text{Ne}$ and $^{31,27}\text{P}$, respectively. Here, the distributions of unstable ^{17}Ne and ^{27}P (displayed by the solid lines) are those of Figs. 2(a) and 2(b), respectively. The proton density distributions of stable ^{20}Ne and ^{31}P nuclei (revealed by the dashed lines) are calculated on the basis that the nucleus ^{20}Ne consists of a core of ^{16}O and the remaining 4 nucleons (2 protons and 2 neutrons) move in the $2s1d$ -model space while the nucleus ^{31}P forms from the core of ^{28}Si and the remaining 3 particles (1 protons and 2 neutrons) move in the HASP-model space. Shell model calculations for ^{20}Ne and ^{31}P are then performed using USD [35] and HASP [42] effective interactions, respectively. The harmonic oscillator size parameters b are chosen so as to reproduce the experimental rms proton radii of stable ^{20}Ne and ^{31}P nuclei. Here, we choose $b = 1.892$ and 1.885 fm for stable ^{20}Ne and ^{31}P nuclei, respectively.

It is so clear from Fig. 3(a) that the proton density distributions of ^{17}Ne

and ^{20}Ne nuclei are diverse even though the two nuclei have the same proton number. As the outer two protons in ^{17}Ne are weakly bound, the proton density distribution of ^{17}Ne has a longer tail than that of ^{20}Ne nucleus. This can be seen obviously from the comparison of the proton density distributions of these nuclei shown in Fig. 3(a). The same argument can be drawn from the proton density distributions of ^{27}P and ^{31}P shown in Fig. 3(b). The weak binding of the last (outer) proton in ^{27}P leads to the extended proton density distribution. This can be noticed visibly from the proton density distributions shown in Fig. 3(b).

To seek out if the long tail behavior of the proton density distribution of the proton-rich nuclei demonstrates noticeable effects in the process of elastic electron scattering, elastic proton form factors for unstable proton-rich (^{17}Ne , ^{27}P) nuclei and their stable isotopes (^{20}Ne , ^{31}P) are calculated by means of the Plane Wave Born Approximation (PWBA).

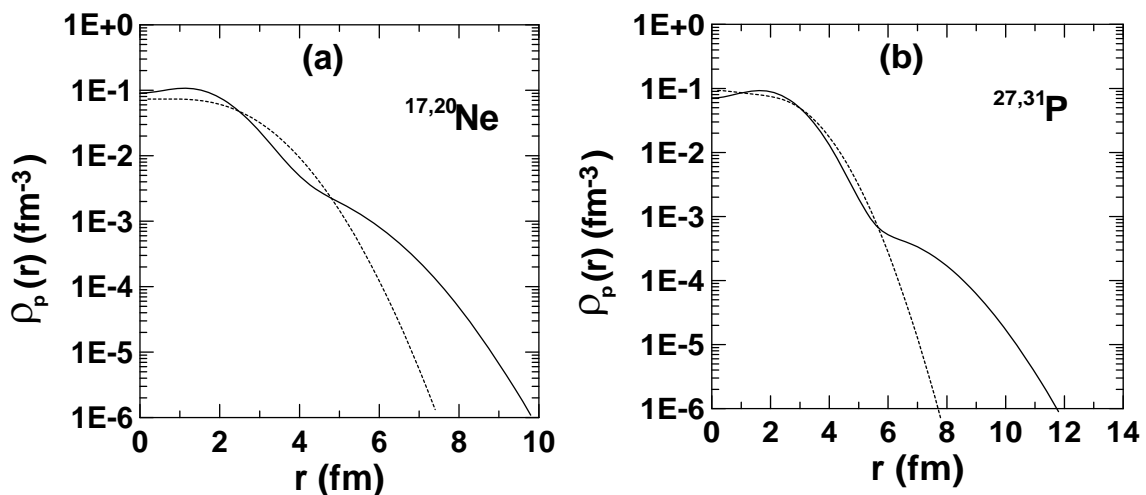


Fig. 3: The dependence of proton density distributions (in fm^{-3}) of $^{20,17}\text{Ne}$ (a) and $^{31,27}\text{P}$ (b) on r (in fm). In (a) and (b), the solid lines are the proton density distributions of ^{17}Ne and ^{27}P whereas the dashed lines are those of stable isotopes ^{20}Ne and ^{31}P .

In Figs. 4(a) and 4(b), we exhibit the dependence of the squared proton form factor $|F(q)|^2$ on the momentum transfer q (in fm^{-1}), where the input proton density distributions are those of Figs. 3(a) and 3(b), respectively. The calculated form factors of the unstable (^{17}Ne , ^{27}P) and stable (^{20}Ne , ^{31}P) nuclei are displayed by the solid and dashed lines, respectively. The experimental elastic charge form factors of stable ^{20}Ne [43] and ^{31}P [44] are displayed by open circles for comparison. Before we investigate the outcome of the long tail behavior of the proton density distribution of unstable ^{17}Ne and ^{27}P on the elastic electron scattering proton form factors, we require examining the validity of the PWBA to the elastic electron-nucleus scattering. For this aim we compare the calculated elastic proton form factors of stable ^{20}Ne and ^{31}P with those of experimental data. Figs. 4(a) and 4(b) demonstrate that both the behavior and the magnitude of the calculated proton form factors (the dashed line) for ^{20}Ne and ^{31}P are in good agreement with all experimental data, where the available data for ^{20}Ne and ^{31}P cover only the range of momentum transfer $q \leq 2 \text{ fm}^{-1}$ and $q \leq 3 \text{ fm}^{-1}$, respectively. However, this comparison gives the conclusion that the PWBA can reproduce the experimental data of elastic electron scattering on the stable ^{20}Ne and ^{31}P .

It is so apparent from Fig. 4(a) that there are important diversities between the calculated form factors of the unstable ^{17}Ne (the solid line) and stable ^{20}Ne (the dashed line). It is clear that each of the solid line and the dashed line has only one diffraction minimum (located at $q = 1.8$ and 1.45 fm^{-1} , respectively) and one maximum (located at $q = 2.15$ and 1.75 fm^{-1} ,

respectively). The position of the diffraction minimum of ^{17}Ne has an outward shift (approximately 0.35 fm^{-1}) as compared with the diffraction minimum of ^{20}Ne . Besides, the amplitude has an important deviation. For a particular momentum transfer $q = 2.15 \text{ fm}^{-1}$, the amplitude deviation of the form factors of ^{17}Ne and ^{20}Ne is nearly $\Delta|F(q)|^2 = 0.302 \times 10^{-3}$.

It is so clear from Fig. 4(b) that there are significant differences between the calculated form factors of ^{27}P (the solid line) and ^{31}P (the dashed line). As we can see that each of the solid line and the dashed line has two diffraction minima (located approximately at $q = 1.4$ and 2.75 fm^{-1} for ^{27}P and at $q = 1.3$ and 2.25 fm^{-1} for ^{31}P) and two maxima (located approximately at $q = 1.7$ and 2.9 fm^{-1} for ^{27}P and at $q = 1.55$ and 2.6 fm^{-1} for ^{31}P). The location of the first and the second minimum of ^{27}P has an outward shift (approximately 0.1 and 0.5 fm^{-1} , respectively) as compared with the first and the second minimum of ^{31}P . The amplitude deviation of the form factors of ^{27}P and ^{31}P at the momentum transfer, for example, $q = 1.7$ and 2.9 fm^{-1} are approximately $\Delta|F(q)|^2 = 0.549 \times 10^{-3}$ and 0.175×10^{-5} , respectively.

As we have mentioned before that the elastic proton form factor in the nucleus is simply connected to its proton density distribution. For that reason, the difference between the proton form factor of ^{17}Ne and that of ^{20}Ne (or ^{27}P and that of ^{31}P) is owing to the different proton density distributions of the two nuclei. Because the difference of the proton density distribution between ^{17}Ne and

^{20}Ne (or between ^{27}P and ^{31}P) is essentially caused by the difference of the proton density distribution of the last two protons in ^{17}Ne and ^{20}Ne (or last proton in ^{27}P and ^{31}P), we attribute the difference between the proton form factor of the unstable and stable nuclei to the different proton density distribution of the last two protons in ^{17}Ne and ^{20}Ne (or of the last proton in ^{27}P and ^{31}P).

To analyze the effect of the long tail of the proton density distributions on elastic electron-nucleus scattering, we require identifying which part of the form factor is responsive to the tail of the proton density distribution. It is recognized from the fitting to the experimental data of ^{12}C [45] and ^{32}S [46] that the form factors in the region of momentum transfer $1 \leq q \leq 3 \text{ fm}^{-1}$

are responsive to the change of the tail part of the proton density distribution, whereas those at the region of high momentum transfer $q \geq 3 \text{ fm}^{-1}$ are responsive to the change of the central part of the proton density distribution. It is expected that the conclusions of ^{12}C [45] and ^{32}S [46] work as well for Ne and P isotopes. Therefore, we may attribute the difference of the calculated form factors at $1 \leq q \leq 3 \text{ fm}^{-1}$ between ^{17}Ne and ^{20}Ne [Fig. 4(a)] and between ^{27}P and ^{31}P [Fig. 4(b)] to the influence of the long tail of the proton density distributions of ^{17}Ne and ^{27}P while those at $q \geq 3 \text{ fm}^{-1}$ to the influence of the proton density differences at the central parts of these isotopes.

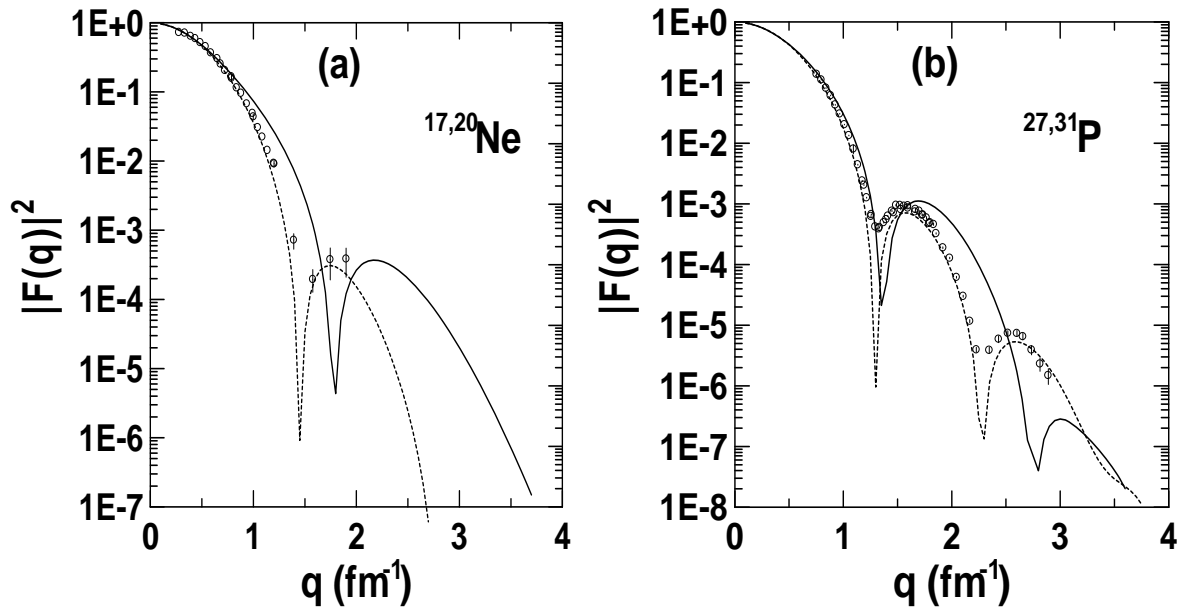


Fig. 4: The dependence of the squared proton form factor $|F(q)|^2$ of $^{17,20}\text{Ne}$ (a) and $^{27,31}\text{P}$ (b) on the momentum transfer q (in fm^{-1}). Here, the input proton density distributions are those of Figs. 3(a) and 3(b), respectively. In (a) and (b), the solid lines are the squared proton form factors of unstable proton-rich ^{17}Ne and ^{27}P nuclei while the dashed lines are those of stable ^{20}Ne and ^{31}P nuclei. The open circles in (a) and (b) are the experimental charge form factors of ^{20}Ne and ^{31}P taken from Refs. [42] and [43], respectively.

Conclusions

The ground state proton, neutron and matter density distributions and corresponding rms radii of unstable proton-rich ^{17}Ne and ^{27}P exotic nuclei are investigated using the two-frequency shell model approach. Elastic electron scattering of these exotic nuclei are also investigated through combining the proton density distribution, obtained by the two-frequency shell model with the PWBA. The long tail behavior, considered as a distinctive feature of halo nuclei, is evidently revealed in the calculated proton and matter density distributions of ^{17}Ne and ^{27}P nuclei. Besides, the noticeable difference that is found between the calculated overall proton and neutron rms radii of ^{17}Ne and ^{27}P nuclei also indicates a definite degree of halo structure. It is found that the structures of ^{17}Ne and ^{27}P nuclei have $(1d_{5/2})^2$ and $2s_{1/2}$ -dominant configurations, respectively. It is also found that the difference between the proton form factor of ^{17}Ne and that of ^{20}Ne (or of ^{27}P and that of ^{31}P) is generally caused by the difference in the proton density distribution of the last two protons (or of the last proton) in the two nuclei. Moreover, it is found that the difference between the proton form factor of the above unstable and stable isotopes at the region $1 \leq q \leq 3 \text{ fm}^{-1}$ is mainly caused by the influence of the long tail behavior presented in the proton density distributions of unstable nuclei while that at the region of $q \geq 3 \text{ fm}^{-1}$ to the influence of the proton density differences at the central parts of these isotopes. Because the difference of the proton form factors between the stable nucleus and its proton drip-line isotope has observable effects, we regard that elastic electron scattering is an

efficient tool to examine proton-halo phenomena of proton-rich nuclei.

Acknowledgments

The authors would like to express their thanks to Professor B. A. Brown of the National Superconducting Cyclotron Laboratory, Michigan State University, for providing the computer code OXBASH.

References

- [1] I. Tanihata, H. Hamagaki, O. Hashimoto, Y. Shida, N. Yoshikawa, K. Sugimoto, O. Yamakawa, T. Kobayashi, N. Takahashi, Phys. Rev. Lett. 55 (1985) 2676.
- [2] I. Tanihata, T. Kobayashi, O. Yamakawa, S. Shimoura, K. Ekuni, K. Sugimoto, N. Takahashi, T. Shimoda, Phys. Lett. B 206 (1988) 592.
- [3] W. Mitting, J. M. Chouvel, Z. W. Long, L. Bianchi, A. Cunsolo, B. Fernandez, A. Foti, J. Gastebois, A. Gillibert, C. Gregoire, Y. Schutz, C. Stephan, Phys. Rev. Lett. 59 (1987) 1889.
- [4] T. Kobayashi, O. Yamakawa, K. Omata, K. Sugimoto, T. Shimoda, N. Takahashi, I. Tanihata, Phys. Rev. Lett. 60 (1988) 2599.
- [5] T. Nilsson, F. Humbert, W. Schwab, H. Simon, M. H. Smedberg, M. Zinser, Th. Blaich, M. J. G. Borge, L.V. Chulkov, Th. W. Elze, H. Emling, H. Geissel, K. Grimm, D. Guillemaud, Mueller, P. G. Hansen, R. Holzmann, H. Imich, B. Jonson, J. G. Keller, H. Klinger, A. A. Korshennikov, J. V. Kratz, R. Kulesa, D. Lambrecht, Y. Leifels, A. Magel, M. Mohar, A. C. Mueller, G. Munzenberg, F. Nickel, G. Nyman, A. Richter, K. Riisager, C. Scheidengerger, G. Schrieder, B. M. Sherrill, K. Stelzer, O. Tengblad, W. Trautmann, E. Wajda, M. V. Zhukov, E. Zude, Nucl. Phys. A 598 (1996) 418.
- [6] M. Zinser, F. Humbert, T. Nilsson, W. Schwab, Th. Blaich, M. J. G.

- Borge, L.V. Chulkov, H. Eickhoff, Th. W. Elze, H. Emling, B. Franzke, H. Freiesleben, H. Geissel, K. Grimm, D. Guillemaud, Mueller, P. G. Hansen, R. Holzmann, H. Imich, B. Jonson, J. G. Keller, O. Klepper, H. Klinger, J. V. Kratz, R. Kulesa, D. Lambrecht, Y. Leifels, A. Magel, M. Mohar, A. C. Mueller, G. Munzenberg, F. Nickel, G. Nyman, A. Richter, K. Riisager, C. Scheidengerger, G. Schrieder, B. M. Sherrill, H. Simon, K. Stelzer, O. Tengblad, W. Trautmann, E. Wajda, E. Zude, Phys. Rev. Lett. 75 (1995) 1719.
- [7] N. A. Orr, N. Anantaraman, Sam M. Austin, C. A. Bertulani, K Hanold, J. H. Kelley, D. J. Morrissey, B. M. Sherrill, G. A. Souliotis, M. Thoennessen, J. S. Winfield, J. A. Winger, Phys. Rev. Lett. 69 (1992) 2050.
- [8] Z. Ren and G. Xu, Phys. Lett. B 252 (1990) 311.
- [9] G. F. Bertsch, and H. Esbensen, Ann. Phys. (N.Y.) 209 (1991) 327.
- [10] M. V. Zhukov, B. V. Danilin, D. V. Fedorov, J. M. Bang, I. J. Thompson, J. S. Vaagen, Phys. Rep. 231 (1993) 151.
- [11] P. G. Hansen, A. S. Jensen, B. Jonson Ann. Rev. Nucl. Part. Sci. 45 (1995) 591.
- [12] J. S. Al-khalili, J. A. Tostevin, I. J. Thompson Phys. Rev. C54 (1996) 1843.
- [13] T. Otsuka, N. Fukunishi, H. Sagawa Phys. Rev. Lett. 70 (1993) 1385.
- [14] Z. Ren, B. Chen, Z. Ma, G. Xu Phys. Rev. C53 (1996) R572.
- [15] B. A. Brown, P. G. Hansen Phys. Lett. B381 (1996) 391.
- [16] A. Navin, D. Bazin, B. A. Brown, B. Davids, G. Gervais, T. Glasmacher, K. Govaert, P. G. Hansen, M. Hellstrom, R. W. Ibbotson, V. Maddalena, B. Pritychenko, H. Scheit, B. M. Sherrill, M. Steiner, J. A. Tostevin, J. Yurkon, Phys. Rev. Lett. 81 (1998) 5089.
- [17] H. Y. Zhang, W. Q. Shen, Z. Z. Ren, Y. G. Ma, W. Z. Jiang, Z. Y. Zhu, X. Z. Cai, D. Q. Fang, C. Zhong, L. P. Yu, Y. B. Wei, W. L. Zhu, Z. Y. Guo, G. Q. Xiao, J. S. Wang, J. C. Wang, Q. J. Wang, J. X. Li, M. Wang., Z. Q. Chen, Nucl. Phys. A 707 (2002) 303.
- [18] R. Morlock, R. Kunz, A. Mayer, M. Jaeger, A. Mueller, J. W. Hammer, P. Mohr, H. Oberhummer, G. Staudt, V. Koelle, Phys. Rev. Lett. 79 (1997) 3837.
- [19] Z. Li, W. Liu, X. Bai, Y. Wang, G. Lian, Z. Li, S. Zeng, Phys. Lett. B 527 (2002) 50.
- [20] H. Y. Zhang, W. Q. Shen, Y. G. Ma, X. Z., Cai, D. Q. Fang, C. Zhong, Y. B. Wei, J. G. Chen, X. F. Zhou, G. L. Ma, K. Wang, Z. Z. Ren, W. L. Zhan, Z. Y. Guo, G. Q. Xiao, H. S. Xu, J. S. Wang, Z. Y. Sun, J. X. Li, M. Wang, Z. Q. Chen, Z. G. Xiao, W. F. Li, J. F. Li, Z. G. Hu, J. Bai, L. x. Chen, Mod. Phys. Lett. A. 18 (2003) 151.
- [21] L. V. Grigorenko, I. G. Mukha, M. V. Zhukov Nucl. Phys. A713 (2003) 372, A740 (2004) 401(E).
- [22] M. V. Zhukov and I. J. Thompson Phys. Rev. C52 (1995) 3505.
- [23] K. Tanaka, M. Fukuda, M. Mihara, M. Takechi, D. Nishimura, T. Chinda, T. Sumikama, S. Kudo, K. Matsuta, T. Minamisono, T. Suzuki, T. Ohtsubo, T. Izumikawa, S. Momota, T. Yamaguchi, T. Onishi, A. Ozawa, I. Tanihata, T. Zheng, Phys. Rev. C 82 (2010) 44309.
- [24] S. Nakamura, V. Guimaraes, S. Kubono Phys. Lett. B416 (1998) 1.
- [25] N. K. Timofeyuk, P. Descouvemont, D. Baye Nucl. Phys. A600 (1996) 1.
- [26] E. Garrido, D. V. Fedorov, A. S. Jensen Phys. Rev. C69 (2004) 24002.
- [27] E. Garrido, D. V. Fedorov, A. S. Jensen Nucl. Phys. A733 (2004) 85.

- [28] H. T. Fortune and R. Sherr Phys. Lett. B503 (2001) 70.
- [29] H. T. Fortune, R. Sherr, B. A. Brown Phys. Rev. C73 (2006) 64310.
- [30] H. Kitagawa, N. Tajima, H. Sagawa Z. Phys. A358 (1997) 381.
- [31] T. Suda, K. Maruyama, I. Tanihata RIKEN Accel. Prog. Rep. 34 (2001) 49, M. Wakasugi, T. Suda, Y. Yano, Nucl. Inst. Meth. Phys. A532 (2004) 216.
- [32] An international accelerator facility for beam of ions and antiprotons, GSI report, 2002.
- [33] B. A. Brown, R. Radhi, B. H. Wildenthal Phys. Rep. 101 (1983) 313.
- [34] E. K. Warburton and B. A. Brown Phys. Rev. C46 (1992) 923.
- [35] B. A. Brown and B. H. Wildenthal Ann.Rev. Nucl. Part. Sci. 38 (1988) 29.
- [36] S. Cohen and D. Kurath Nucl. Phys. A73 (1965) 1.
- [37] T. T. S. Kuo, H. Muether, K. Amir-Azimi-Nili Nucl. Phys. A606 (1996) 15, T T S Kuo, F Krmpotic, and Y Tzeng Phys. Rev. Lett. 78 (1997) 2708.
- [38] A. B. Brown, A. Etchegoyen, N. S. Godin, W. D. M. Rae, W. A. Richter, W. E. Ormand, E. K. Warburton, J. S. Winfield, L. Zhao, C. H. Zimmermam, MSU-NSCL Report Number 1289 (2005).
- [39] A. Ozawa, I. Tanihata, T. Kobayashi, Y. Sugahara, O. Yamakawa, K. Omata, K. Sugimoto, D. Olson, W. Christie, H. Wieman, Nucl. Phys. A 608 (1996) 63.
- [40] A. Ozawa, T. Kobayashi, H. Sato, D. Hirata, I. Tanihata, O. Yamakawa, K. Omata, K. Sugimoto, D. Olson, W. Christie, H. Wieman, Phys. Lett. B 334 (1994) 18.
- [41] D. Q. Fank, W. Q. Shen, J. Feng, X. Z. Cai, H.Y. Zhang, Y. G. Ma, C. Zhong, Z. Y. Zhu, W. Z. Jiang, W. L. Zhan, Z. Y. Guo, G. Q. Xiao, J. S. Wang, J. Q. Wang, J. X. Li, M. Wang, J. F. Wang, Z. J. Ning, Q. J. Wang, Z. Q. Chen, Eur. Phys. J. A 12 (2001) 335.
- [42] H. Hasper, Phys. Rev. C19 (1979) 1482.
- [43] E. A. Knight, R. P. Singhal, R. G. Arthur, M. W. S. Macauley, J. Phys. G: Nucl. Phys. 7 (1981) 1115.
- [44] J. Wesseling, C. W. de Jager, L. Lapikas, H. de Vries, Phys. Rev. C55 (1997) 2773.
- [45] I. Sick and J. S. McCarthy Nucl. Phys. A150 (1970) 631.
- [46] G. C. Li, M. R. Yearian, I. Sick Phys. Rev. C9 (1974) 1861.